Impact of magnetic ripple on neoclassical equilibrium in gyrokinetic simulations

R Varennes, X Garbet, L. Vermare, Y Sarazin, Guilhem Dif-Pradalier, V Grandgirard, P Ghendrih, P Donnel, M Peret, K Obrejan, et al.

PAPER

Impact of magnetic ripple on neoclassical equilibrium in gyrokinetic simulations

IOP Publishing Plasma Physics and Controlled Fusion
Plasma Phys. Control. Fusion **65** (2023) 035016 (16pp) https://doi.org/10.1088/1361-6587/acb79a

Impact of magnetic ripple on neoclassical equilibrium in gyrokinetic simulations

R Varennes[1,*], X Garbet[1], L Vermare[2], Y Sarazin[1], G Dif-Pradalier[1], V Grandgirard[1], P Ghendrih[1], P Donnel[1], M Peret[1], K Obrejan[1] and E Bourne[1]

[1] CEA, IRFM, F-13108 Saint-Paul-Lez-Durance, France
[2] LPP, CNRS, Ecole polytechnique, 91128 Palaiseau, France

E-mail: robin.varennes@gmail.com

Received 8 April 2022, revised 19 December 2022
Accepted for publication 31 January 2023
Published 9 February 2023

Abstract

The effect of magnetic field ripple on tokamak plasma without turbulence is studied numerically and augmented with a reduced analytical model that includes neoclassical processes in the presence of non-axisymmetric perturbation and stochastic transport. For this study, a magnetic field ripple perturbation has been implemented in the GYSELA gyrokinetic code. This implementation has been verified thanks to a test of toroidal angular momentum conservation. The GYSELA code was then successfully benchmarked against the NEO code, which solves the drift kinetic equation, and against the reduced model in the collisionality range $\nu^\star \in [0.05\text{–}0.5]$ for several amplitudes of the magnetic ripple. An observation, shared by the model, the NEO code and GYSELA simulations is that the thermal drive of the mean poloidal velocity—measured by the k_{V_P} coefficient—decreases sharply for large yet experimentally relevant magnetic ripple amplitudes, and may even change sign.

Keywords: neoclassical transport, stochastic transport, plasma flow, full-f gyrokinetic simulations

(Some figures may appear in colour only in the online journal)

1. Introduction

The impact of non-axisymmetric magnetic perturbations on flows is of prime importance to understand confinement. This is particularly true for stellarators. However tokamaks also exhibit such perturbations which can fundamentally modify transport even at small amplitudes [1, 2]. Here special attention is paid to the magnetic field *ripple*, caused by the discrete number of toroidal coils. Magnetic ripple impacts transport by modifying both neoclassic and turbulent transport. Only the former is studied here, while the impact of turbulent effects is described in [3]. In the absence of turbulence, magnetic ripple modifies the particle trajectories in many ways. First, magnetic ripple causes a loss of axisymmetry of the system and therefore of the associated invariant of motion: the canonical toroidal momentum. Confinement is then breached, leading to non-vanishing radial transport as a result of the local toroidal trapping that occurs between two consecutive toroidal coils. Particles trapped in these magnetic wells undergo vertical magnetic drift that is not compensated anymore by the motion along the helical magnetic field lines (except in the presence of strong E×B drift). Consequently, ripple can lead to transport even in collisionless plasmas. Secondly, neoclassical effects, i.e. collisional processes enhanced by particle trajectories, are substantially changed and modify flows in consequence. In particular, a well-established result of the neoclassical theory in an axisymmetric magnetic configuration is the degeneracy between the toroidal velocity V_T and the radial electric field E_r. Ripple breaks axisymmetry and forces V_T and E_r to converge toward well-defined values. Finally, non-turbulent stochastic transport can arise above a ripple amplitude threshold. Particles then describe a

* Author to whom any correspondence should be addressed.

chaotic motion resulting in an effective diffusion that leads to transport.

The accurate simulation of these transport properties requires a kinetic approach. To study these effects, magnetic field ripple has been implemented in the gyrokinetic code GYSELA [4]. In this study, this implementation is verified thanks to the toroidal momentum conservation equation since ripple is responsible for an additional toroidal torque, usually called *Neoclassical Toroidal Viscosity* [5, 6]. The ripple implementation is then confronted with a reduced analytical model of neoclassical [7] and stochastic loss [8] physics. Good agreement is found on neoclassical transport coefficients used to predict the toroidal velocity, the poloidal velocity and the radial electric field. A benchmark with the drift-kinetic solver NEO [9, 10] is also performed and found in fair agreement with GYSELA results. A peculiar additional observation, shared by GYSELA, NEO and the analytical model is the strong effect of ripple on the poloidal velocity even for typical tokamak ripple amplitudes.

The rest of this paper is organized as follows. Neoclassical and stochastic transport mechanisms in the presence of ripple perturbation are recalled in section 2. where the model is defined. The predictions of the model on flows are compared with asymptotic studies in section 3. The numerical model of the GYSELA code is presented in section 4. In section 5, the verification of the implementation of the magnetic perturbation in GYSELA is detailed. Then, neoclassical theoretical predictions are compared with GYSELA and NEO simulations in section 6. The modification of the poloidal velocity by neoclassical effects with ripple is discussed in section 7. A summary is given in section 8.

2. Theoretical neoclassical predictions

In this study, a simplified geometry is considered where magnetic surfaces are taken circular and concentric. In toroidal coordinates (r,θ,φ), and in the limit of large aspect ratio and small ripple magnitude, the magnetic field amplitude B can be approximated as follows:

$$B = B_0(1 - \underbrace{\varepsilon(r)\cos\theta}_{\text{1/R decay}} + \underbrace{\delta(r,\theta)\cos(N_c\varphi)}_{\text{magnetic ripple}}). \quad (1)$$

Here, B_0 is a reference magnetic field amplitude taken on the magnetic axis and in between two coils, $\varepsilon = r/R_0$ with R_0 the major radius, δ is the ripple amplitude and N_c the number of toroidal coils. The $1/R$ magnetic field decay is responsible for banana trapping. Ripple is also responsible for so-called local trapping in between two consecutive toroidal coils that create a magnetic well where particles can bounce back and forth. Without turbulence, particle motion is constrained by the magnetic configuration and collisions. Those constraints account for neoclassical and stochastic transport. The derivation of the neoclassical part heavily relies on the existence of invariants of motion that are not valid with chaos. Consequently, in order to have consistency in the complete model, the neoclassical part is considered to hold only in the adiabatic limit $N_c\Omega_D \ll \Omega_B$ where Ω_D and Ω_B are the precession and banana-bounce frequencies. The origin of this limit is explained below. Let us detail the neoclassical and stochastic aspects separately.

First, neoclassical transport at low collisionality is due to the resonant enhancement of collisional processes. It owes its existence to trapped particles. Indeed, in the vicinity of bounce points, the particle parallel velocity $v_\parallel$ vanishes and the magnetic drift becomes dominant; this corresponds to the resonance. Now, if the plasma is collisionless, transport can only occur if particle trajectories are not confined. It is possible with magnetic field ripple as particles trapped between two coils undergo a vertical magnetic drift which is not compensated by the motion along the magnetic field lines. In the axisymmetric case, there would be no transport at all. Adding collisions to this problem accounts for the so-called neoclassical theory. When the collision frequency becomes comparable to the bounce frequency of the considered trapped population, a random walk with a characteristic step linked to the resonance prevails. Considering banana trapping for example, this step would be roughly the banana width. Subtleties also appear when accounting for the synergies between the different trappings. For example, the ripple causes banana bounce points to drift radially in such a way that they undergo a random walk process. The reduced model is meant to describe all those processes. It relies on a kinetic derivation of the equilibrium distribution function for the considered species. Each population (trapped or passing) tends to relax toward a Maxwellian equilibrium under the effect of collisions. The resulting total distribution function can however be non-Maxwellian and therefore leads to finite fluxes.

This physics is captured by the gyrokinetic code GYSELA. Figure 1 shows the impact of the $1/R$ magnetic field decay and magnetic ripple on the distribution function in the $(\theta, v_\parallel)$ and $(\varphi, v_\parallel)$ spaces. Magnetic ripple produces islands in the $(\varphi, v_\parallel)$ space corresponding to particles trapped toroidally between coils. The island in the $(\theta, v_\parallel)$ space, corresponding to the banana trapping, is also modified with ripple. As discussed previously, the effect is maximum at $v_\parallel = 0$ where the resonance takes place. A similar mechanism also exists for particles in ripple wells.

To get the expression of the distribution function and associated transport, one must start with the drift kinetic equation (DKE). The first step of the derivation then relies on solving the DKE for each perturbation, i.e. the $1/R$ magnetic field decay or ripple, independently. They are labeled 'primary' perturbations. Solving the DKE with the $1/R$ magnetic field decay as primary perturbation leads to the axisymmetric neoclassical theory. Doing the same for the ripple perturbation amounts to consider collisional processes in a tokamak without curvature, i.e. a rippled cylinder, with equally spaced coils leading to local trapping. The next step is to perturb the trapped population by the primary perturbation with the other one, labeled 'secondary' perturbation. If ripple is the secondary perturbation, it then accounts for the radial drift of the banana bounce point induced by ripple. If the $1/R$ magnetic field decay is the secondary perturbation, it then accounts for the bounce points of the ripple-induced trapped trajectories drifting vertically due to the magnetic curvature drift. Those

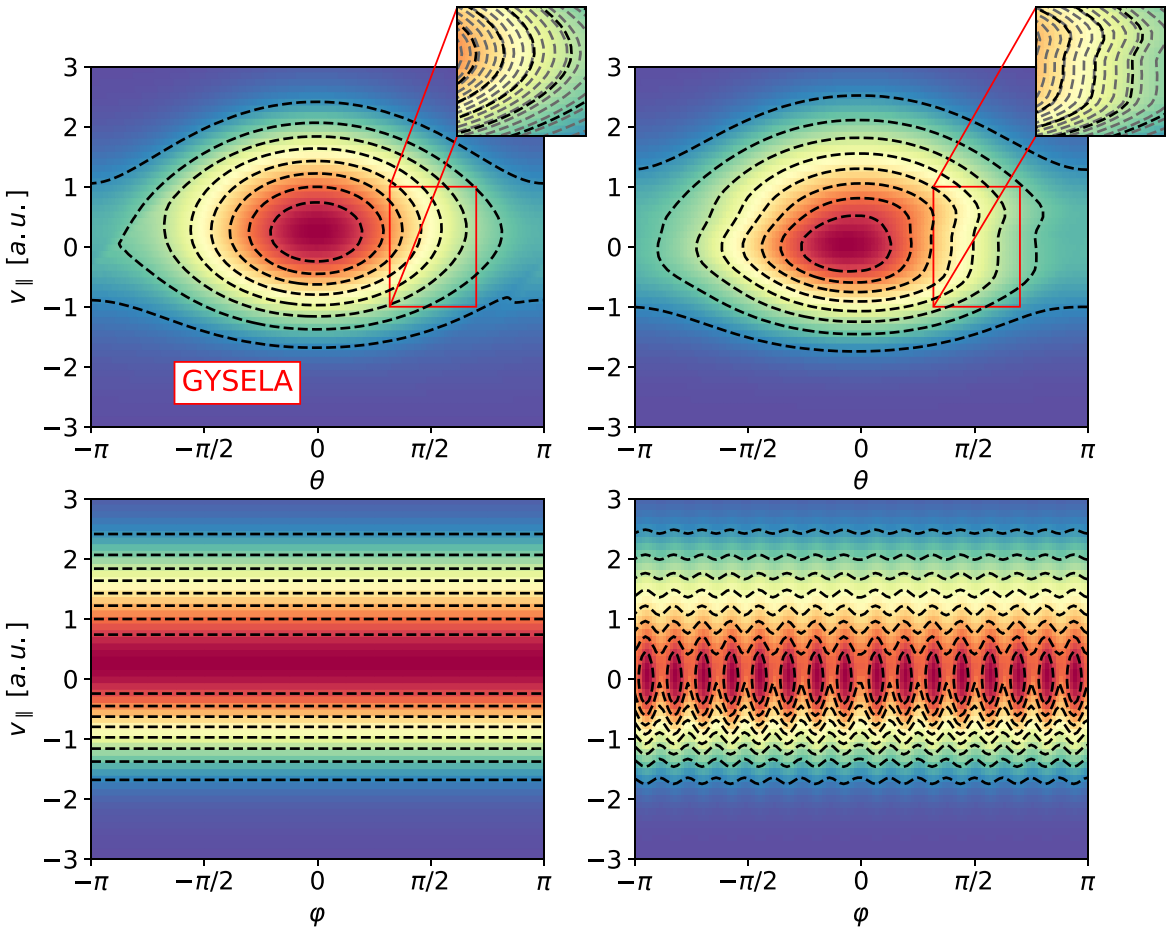

Figure 1. Distribution function of trapped particles without (left) and with (right) ripple, obtained with GYSELA, with $N_c = 16$. Ripple accounts for an additional trapping in the toroidal direction and also modifies the island of banana trapped particles near bounce points.

four contribution branches to neoclassical transport can be summed up in this list [11]:

- the *axisymmetric branch* is the neoclassical contribution of unperturbed banana particles;
- the *helically symmetric branch* is the neoclassical contribution of unperturbed ripple-induced trapping;
- the *banana drift branch* is the neoclassical contribution from ripple effect on banana trapped particles;
- the *ripple-wells drift branch* is the neoclassical contribution from the $1/R$ magnetic field decay effect on particles trapped in ripple-induced magnetic wells.

Let us now talk about stochastic transport. It refers to a collisionless diffusion that can arise in the presence of ripple for some banana-trapped particles. Here is the principle. As mentioned before, ripple causes a radial jump Δr of the banana-trapped particles at the bounce point locations. This jump is either inward or outward depending on the relative toroidal angle φ_B of the bounce point relative to the two nearest coils. It can be expressed as $\Delta r = \lambda \rho_i \delta \cos(N_c \varphi_B - \pi/4)$ where $|\lambda| \sim \sqrt{N_c}(q/\varepsilon)^{3/2}$ [12] with q the safety factor and φ_B the toroidal angle of bounce points. In most tokamaks, an estimate at the edge is $\sqrt{\langle \Delta r^2 \rangle_\varphi} \sim 2 - 3\rho_i$ where $\langle . \rangle_\varphi$ is the toroidal average. If $\Delta r > 0$ (outward) in between two coils, then $\Delta r < 0$ (inward) in the vicinity of the coils. As trapped particles drift toroidally at the precession frequency Ω_D, they undergo a different radial shift at each bounce point. After each bounce period $2\pi/\Omega_B$, one can define a toroidal phase shift $\Delta\varphi_B = \varphi_B(t - 2\pi/\Omega_B) - \varphi_B(t)$. If $\Delta\varphi_B$ is small with respect to the toroidal angle span separating two coils $\Delta\varphi_C = 2\pi/N_C$, the consecutive radial shifts exerted on the particle are expected to be as often inward as outward, resulting in a zero mean radial displacement. However, in the other limit, namely $N_C\Omega_D \gg \Omega_B$, $\Delta\varphi_B$ becomes comparable to $\Delta\varphi_C$. In this scenario, consecutive bounce point positions follow no particular order and stochasticity appears. This mechanism is illustrated in figure 2.

The whole analytical calculation of neoclassical and stochastic transport is a formidable task that will not be detailed in this paper. The interested reader can look at [11, 13–23] for the neoclassical part and at [8, 12, 24] for the stochasticity part. The model considered in this paper is based on the review by Garbet *et al* [7] on top of which stochastic transport has been added. It leads to a transport matrix that links the equilibrium fluxes of particles Γ and heat Q as well as the magnetic drag force $\mathcal{M}$ with the thermodynamic gradient forces, the mean toroidal velocity V_T and the radial electric

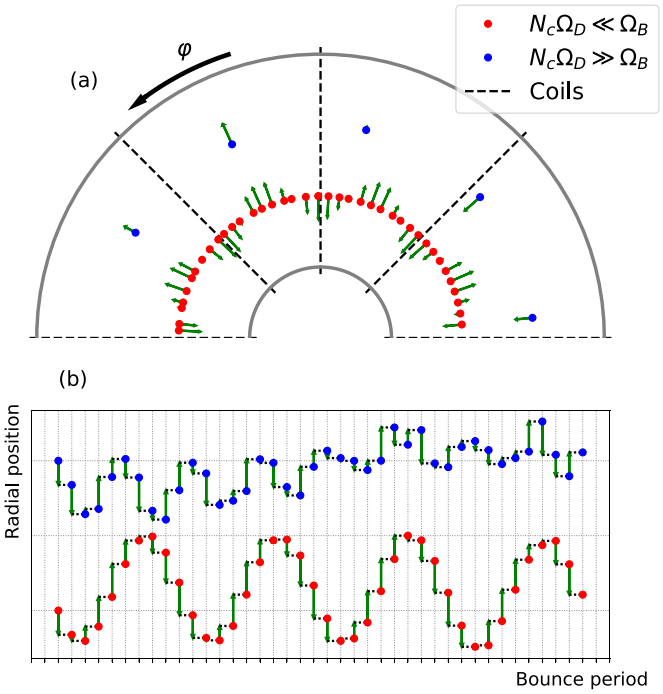

Figure 2. (a) Schematic view in toroidal section of bounce point for trapped particles either below the stochasticity limit (red) or above (blue). Green arrow shows the direction and amplitude of the radial shift Δr exerted on particle by ripple. (b) Successive radial positions of the bounce point for each case.

field E_r. For a single ion species, it can be expressed in this compact way:

$$\begin{pmatrix} \Gamma_N \\ \Gamma_{V_T} \\ \Gamma_T \end{pmatrix} = -D_P \begin{pmatrix} d_0+\tilde{d}_0 & d_0 & d_1+\tilde{d}_1 \\ d_0 & d_0+\hat{d}_0 & d_1 \\ d_1+\tilde{d}_1 & d_1 & d_2+\tilde{d}_2 \end{pmatrix} \cdot \begin{pmatrix} A_N \\ A_{V_T} \\ A_T \end{pmatrix} \tag{2}$$

where $\Gamma_N = \frac{\Gamma}{n}$, $\Gamma_{V_T} = \frac{\mathcal{M}}{neB_p}$, $\Gamma_T = \frac{Q}{nT}$, $A_N = \frac{1}{n}\frac{dn}{dr} - \frac{eE_r}{T}$, $A_{V_T} = \frac{eB_p}{T}V_T$, $A_T = \frac{1}{T}\frac{dT}{dr}$ with n the density, T the temperature, e the electric charge and B_P the poloidal component of the magnetic field. $D_P = \frac{qR_0}{V_{\text{thi}}}\left(\frac{T}{eB_0R_0}\right)^2$ is a reference diffusion coefficient, where $V_{\text{thi}} = \sqrt{T/m}$ is the ion thermal velocity and q the safety factor.

The transport matrix coefficients are detailed in appendix A. They only depend on three dimensionless parameters: $\nu^\star$, δ/ε and $N_c q$ (with q the safety factor). The coefficients d_i are independent of δ/ε. Without ripple, i.e. $\tilde{d}_i = 0$ and $\hat{d}_i = 0$, one recovers the classic coefficients resulting from the axisymmetric neoclassical theory at lower order in ε. In that case, it is clear that the two first lines of the transport matrix are identical. This degeneracy explains why axisymmetric neoclassical theory cannot predict A_N and A_{V_T} independently, and hence treats the radial electric field and the toroidal velocity as a single unknown.

3. Flow predictions with the analytical model

In this section, the previous model is used to predict meaningful quantities relevant to the plasma flow, and is compared with common asymptotic regimes. Let us first define these 'meaningful quantities'. First, there are thermal drive coefficients that link the equilibrium toroidal velocity $V_{T,\text{eq}}$, poloidal velocity $V_{P,\text{eq}}$ and the radial electric field $E_{r,\text{eq}}$ to the temperature gradient, labeled k_{V_T}, k_N and k_{V_P} respectively. The thermal drive coefficient expressions are obtained when considering that both Γ_N and Γ_{V_T} go to zero at equilibrium (without external sources of particles and momentum).

Under these conditions, equation (2) gives the equalities

$$k_{V_T}\frac{\nabla T_{\text{eq}}}{eB_P} = V_{T,\text{eq}} \tag{3}$$

$$k_{V_P}\frac{\nabla T_{\text{eq}}}{eB_T} = V_{P,\text{eq}} \tag{4}$$

$$k_N\frac{\nabla T_{\text{eq}}}{T_{\text{eq}}} = \frac{eE_{r,\text{eq}}}{T_{\text{eq}}} - \frac{\nabla n_{\text{eq}}}{n_{\text{eq}}} \tag{5}$$

where the 'eq' subscript denotes values taken at equilibrium and B_T,B_P are the toroidal and poloidal components of the magnetic field $\boldsymbol{B}$.

These equations can also be written in an dimensionless form:

$$A_{V_T} = k_{V_T}A_T \tag{6}$$

$$A_{V_P} = k_{V_P}A_T \tag{7}$$

$$A_N = -k_N A_T. \tag{8}$$

The explicit expressions of the thermal drives when these two fluxes vanish are

$$k_{V_T} = \frac{d_0\tilde{d}_1 - d_1\tilde{d}_0}{(d_0+\tilde{d}_0)(d_0+\hat{d}_0) - d_0^2} \tag{9}$$

$$k_N = \frac{(d_0+\hat{d}_0)(d_1+\tilde{d}_1) - d_0d_1}{(d_0+\tilde{d}_0)(d_0+\hat{d}_0) - d_0^2} \tag{10}$$

$$k_{V_P} = 1 + k_{V_T} - k_N \tag{11}$$

where the thermal drive k_{V_P} has been obtained with the force balance equation $A_{V_P} = \frac{eB_T}{T}V_P = A_N + A_{V_T} + A_T$. This force balance is used as a constraint, but note that this model solves a kinetic transport equation and thus treats the toroidal and poloidal components of the velocity self-consistently. Knowing those thermal drive coefficients as well as the temperature gradient, one can make predictions on the final flow.

These coefficients are commonly considered in some asymptotic regimes of collisionality and ripple amplitude. These regimes depend among others on the parameter $Y(r,\theta) = \frac{\varepsilon|\sin\theta|}{\delta N_c q}$. Regions with $Y < 1$ are characterized by local magnetic wells in between two toroidal field coils. Conversely,

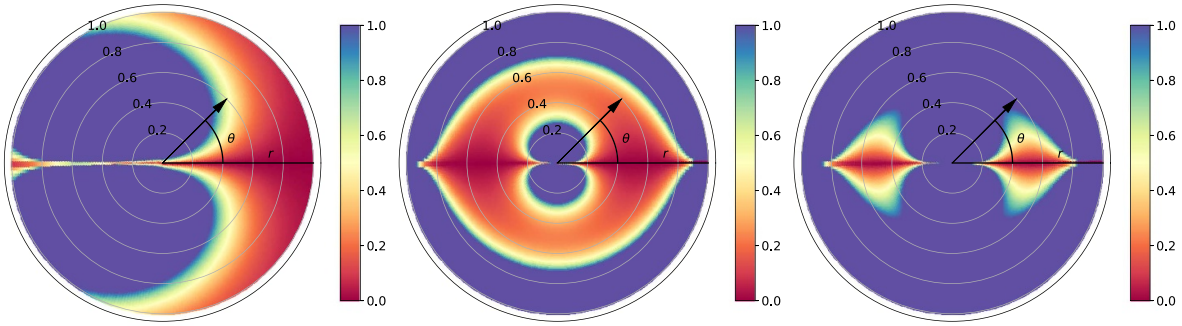

Figure 3. Condition of existence of ripple-induced magnetic wells in the Tore Supra tokamak (a) a radially gaussian ripple centered at mid-radius and poloidally symmetric with a $\delta = 3\%$ peak (b) and a $\delta = 0.5\%$ peak (c). There are no magnetic wells in $Y > 1$ areas (blue) so no local trapping can occur.

Table 1. Asymptotic values of k_{V_T}, k_N and k_{V_P} for different ranges of δ/ε, $\nu^\star$ and $N_c q$.

	$Y > 1$		$Y < 1$ (Local mirrors)		$\forall Y$
	$\forall \delta/\varepsilon$		$\delta/\varepsilon < 1$	$\delta/\varepsilon > 1$	$\forall \delta/\varepsilon$
	$\nu^\star \ll (N_c q)^{-2}$	$(N_c q)^{-2} \ll \nu^\star \ll 1$	$\nu^\star < (\delta/\varepsilon)^{3/2}$	$\nu^\star < 1$	$\nu^\star \gg 1$
k_N	3.37	1.5	3.37	3.37	1.5
k_{V_P}	1.17	1.17	1.17	−2.37	−0.5
k_{V_T}	3.54	1.67	3.54	0.0	0.0

for $Y > 1$, such magnetic wells do not exist so there is no ripple-induced trapping in those regions.

This subtle point is worth discussing as predictions are significantly different between regions with or without ripple-induced magnetic wells. It indicates that a poloidal dependence must be taken into account. Indeed, for the same ripple amplitude but different ripple shapes, the thermal drive predictions can be different. For this reason, and for numerical convenience explained below, the considered ripple perturbation for this academic work is poloidally symmetric. Figure 3 displays the poloidal map of Y for the Tore Supra tokamak and for two radially gaussian ripple amplitude profiles centered at mid-radius. That said, the asymptotic regimes of k_{V_T}, k_N and k_{V_P} are summarized in table 1.

In this table, one can observe that thermal drive coefficients change substantially depending on collisionality regimes. For example, k_{V_T} can double in regions without magnetic wells under the sole effect of collisionality. It means that for a given temperature gradient, the toroidal velocity can change drastically when the collisionality evolves (due to heating for example). Similar effects can be observed for k_N and k_{V_P}. However, this table can easily be misleading for several reasons. First, the model is poloidally averaged so the resulting thermal drive can be a mix between their predictions in $Y > 1$ regions and $Y < 1$ regions. Then, those asymptotic regimes hide that those thermal drives actually depend non-linearly on δ/ε and $\nu^\star$. Consequently, the transition between those regimes has no reason to be smooth or even monotonous.

Although less accurate than simulation codes, the reduced model has the advantage over simulation codes to provide transport coefficients effortlessly. In other words, it can be used to perform scans on wide ranges of δ/ε, $\nu^\star$ and $N_c q$. Now and for the remaining of the paper, a fixed $N_c q = 16 \times 1.4$ is considered. The thermal drive coefficients k_{V_T}, k_N or k_{V_P} are scanned for the ranges of δ/ε and $\nu^\star$ as shown in figure 4.

All asymptotic regimes are recovered. It should be mentioned however that the so-called Pfirsch–Schlüter regime is expected to play a role for $\nu^\star \gg 10$. This regime is not included in the model and is expected to change k_{V_P} toward even more negative values [25] (indeed the prediction in axisymmetric configuration is $k_{V_P} \to -2.1$). The transitions between the different regimes are mainly due to the $(\delta/\varepsilon)^{-1}$ dependence of Y. Indeed, as (δ/ε) increases, the size of the regions where ripple-induced magnetic wells exist also increases. In the range of the (δ/ε) parameter where the $Y < 1$ regions become dominant compared with $Y > 1$ regions, important variations of k_{V_T}, k_N and k_{V_P} are observed. In particular, k_{V_P} decreases toward negative values with increasing ripple amplitude. Section 7 of this document is dedicated to a discussion of this effect. In section 6, these observations, obtained with the analytical model, are confronted to the simulation codes GYSELA and NEO.

Another interesting quantity can be defined to assess the dynamics of the toroidal flow: the neoclassical toroidal friction ν_φ. It corresponds to the characteristic relaxation frequency—set by ripple-induced neoclassical processes—of the toroidal flow toward its predicted equilibrium value (governed by k_{V_T}). Regarding the analytical model, this quantity appears when a situation out of equilibrium is considered. Subtracting the second line from the first one in equation (2) reads

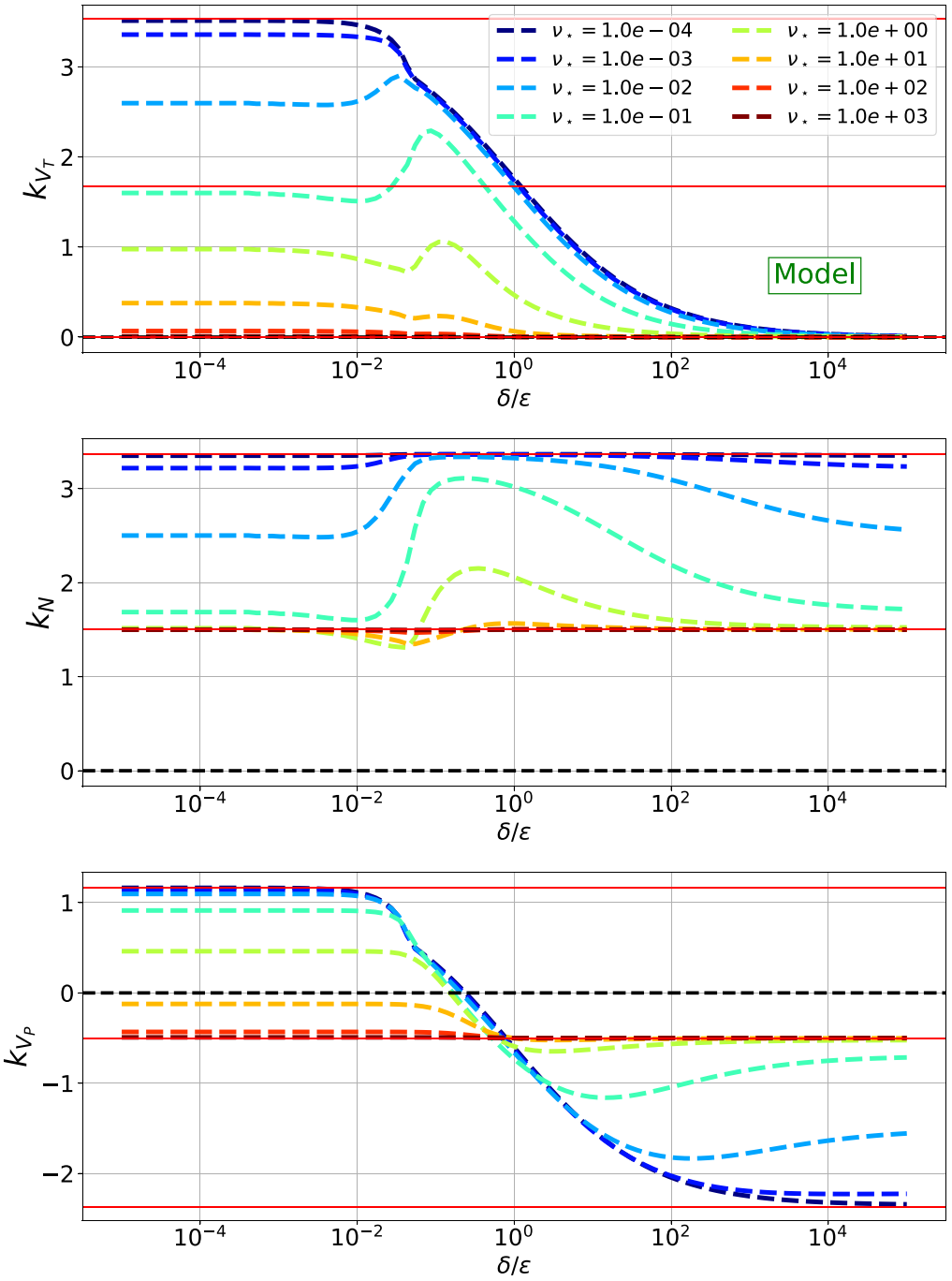

Figure 4. Scan in ripple amplitude of thermal drives k_{V_T}, k_N and k_{V_P} for a wide range of $\nu^\star$. Red plain lines represent the asymptotic values that appear in table 1.

$$\Gamma_{V_T} - \Gamma_N = -D_P \left(\hat{d}_0 A_{V_T} - \tilde{d}_0 A_N - \tilde{d}_1 A_T \right). \tag{12}$$

The resulting neoclassical toroidal friction ν_φ is then the coefficient that multiplies A_{V_T}. Its expression significantly changes depending on the assumptions taken on the fluxes. Indeed, if one considers that neither the particle flux nor the momentum flux vanishes in this out-of-equilibrium situation, i.e. $\Gamma_N \neq 0$ and $\Gamma_{V_T} \neq 0$, the neoclassical friction then reads $\nu_\varphi = \hat{d}_0$.

However, keeping the ambipolarity constraint $\Gamma_N = 0$ but with a finite momentum flux, i.e. $\Gamma_{V_T} \neq 0$, equation (2) gives $\Gamma_{V_T} = -D_P \nu_\varphi^{\Gamma_N=0} (A_{V_T} - k_{V_T} A_T)$ with

$$\nu_\varphi^{\Gamma_N=0} = \hat{d}_0 + \frac{d_0 \tilde{d}_0}{d_0 + \tilde{d}_0}. \tag{13}$$

Notice that, since $\hat{d}_0$ and $\tilde{d}_0$ go to zero when $\delta/\varepsilon \to 0$, the neoclassical friction always (i.e. regardless of the

assumption on the fluxes) vanishes in the axisymmetric case as a consequence of the degeneracy: without ripple the toroidal velocity does not relax toward any prescribed value. Furthermore, $\hat{d}_0$ and $\tilde{d}_0$ increase with δ/ε so that the system relaxes faster with higher ripple amplitude, as one would expect on the basis of qualitative physical arguments. In section 6, the neoclassical friction is assessed with the GYSELA code. Documentation on this neoclassical friction can be found in references focused on externally applied magnetic perturbations [26–29]. However, none of the references known to the authors actually clearly addresses this neoclassical toroidal friction due to magnetic ripple in tokamaks, neither through analytical study nor numerical simulations.

4. Ripple implementation in GYSELA

The aim of this section is to recall the basic set of equations of the GYSELA code and explain how magnetic ripple is implemented. A detailed description of the GYSELA code can be found in Grandgirard *et al* [4]. In the electrostatic regime considered in this paper, GYSELA solves a kinetic equation per considered species coupled to the quasi-neutrality constraint. The gyrokinetic Fokker-Planck equation associated with each species s reads:

$$\frac{\partial \bar{F}_s}{\partial t} + \frac{d\mathbf{x}_G}{dt}\cdot\boldsymbol{\nabla}\bar{F}_s + \frac{dv_{G\|}}{dt}\frac{\partial \bar{F}_s}{\partial v_{G\|}} = \mathcal{C}(\bar{F}_s) \tag{14}$$

where $\mathbf{x}_G$ and $v_{G\|}$ are the position and velocity of the gyrocenter, $\bar{F}_s$ is the gyrocenter distribution function, and $\mathcal{C}$ is a collision operator.

The electrostatic quasi-neutrality equation (15), here expressed in the case of adiabatic electrons and in the limit of long wavelengths (with respect to the thermal ion Larmor radius), reads:

$$\begin{aligned}\frac{e\left[\phi-\langle\phi\rangle\right]}{T_e} - \sum_s \frac{1}{n_{\mathrm{eq},s}}\nabla_\perp\cdot\left[\frac{m_s n_{\mathrm{eq},s}}{e_s B^2}\nabla_\perp\phi\right] \\ = \sum_s \frac{1}{n_{\mathrm{eq},s}}\iint \frac{2\pi B^\star_{\|,s}}{m_s} dv_{G\|}d\mu\mathcal{J}(\bar{F}_s-\bar{F}_{\mathrm{eq},s})\end{aligned} \tag{15}$$

where $\langle.\rangle$ denotes a flux-surface average, $\mathcal{J}$ is the gyroaverage operator, ϕ is the electric potential, T_e is the electron temperature and e the ion charge. For each ion species s, m_s is the mass, e_s is the charge and $B^\star_{\|,s}$ is the Jacobian of the coordinate transform. The density $n_{\mathrm{eq},s}$ is calculated with the equilibrium Maxwellian gyroaveraged distribution function $\bar{F}_{\mathrm{eq},s}$. This is the set of equations solved in the simulation code GYSELA.

The current version of the GYSELA code uses a set of toroidal coordinates labeled $\{x^i\} = (r,\theta,\varphi)$, where r is the radial position, θ the poloidal geometric angle, and φ the toroidal angle. In this paper, the magnetic surfaces are set circular and concentric such that the Jacobian in space reads $\mathcal{J}_x = rR$ where $R(r,\theta) = R_0 + r\cos\theta$. The axisymmetric magnetic field $\mathbf{B}$ is defined as

$$\mathbf{B} = \frac{B_0R_0}{R(r,\theta)}\left[\frac{r}{q(r)R_0}\hat{\mathbf{e}}_\theta + \hat{\mathbf{e}}_\varphi\right] \tag{16}$$

where $\hat{\mathbf{e}}_\theta = r\boldsymbol{\nabla}\theta$ and $\hat{\mathbf{e}}_\varphi = R\boldsymbol{\nabla}\varphi$ are unit vectors in the poloidal and toroidal periodic direction respectively, and q is the safety factor. In this case, the electrostatic gyrokinetic equations of motion solved in GYSELA are

$$B^\star_\| \frac{d\mathbf{x}_G}{dt} = v_{G\|}\mathbf{B}^\star + \frac{\mathbf{b}}{e_s}\times\boldsymbol{\nabla}\mathcal{H} \tag{17}$$

$$B^\star_\| m_s \frac{dv_{G\|}}{dt} = -\mathbf{B}^\star\cdot\boldsymbol{\nabla}\mathcal{H} \tag{18}$$

where $\mathbf{b} = \mathbf{B}/B$ is the unit vector parallel to the magnetic field direction, $\mathbf{B}^\star = \mathbf{B} + \frac{m_s v_{G\|}}{e_s}\boldsymbol{\nabla}\times\mathbf{b}$ and $\mathcal{H} = \frac{m_s}{2}v^2_{G\|} + \mu_s B + e_s\mathcal{J}[\phi]$ is the axisymmetric Hamiltonian, with ϕ the electric potential. In principle, the ripple perturbation $\delta\mathbf{B}$ should be included by modifying both the magnetic field vector $\mathbf{B}$ and its modulus. Modifying the vector $\mathbf{B}$ in such a heavy code is very challenging. Indeed, adding a toroidal component to the magnetic field would change the magnetic surface shape such that the metrics would become 3D. This tremendous work is unnecessary, as modifying only the Hamiltonian is sufficient for acceptable accuracy. Indeed, it can be shown that this simplification changes the expression of the magnetic braking torque $\mathcal{M}_s$, which is the main effect of ripple, from $\mathcal{M}_s = -\int d^3\mathbf{v}F_s\left\{(m_s v^2_{G\|} + \mu_s B)R\frac{(\hat{\mathbf{e}}_\varphi\cdot\boldsymbol{\nabla})B}{B}\right\}$ to $\mathcal{M}_s = -\int d^3\mathbf{v}F_s\{\mu_s R(\hat{\mathbf{e}}_\varphi\cdot\boldsymbol{\nabla})B\}$. At low collisionality, magnetic ripple impacts mainly the trapped particles so the error on $\mathcal{M}_s$ can not exceed ε for banana-trapped particles and δ for locally trapped particles. This reasonable assumption is detailed in [30] that discusses the non-axisymmetric perturbation implementation in the gyrokinetic code GT5D. The new effective Hamiltonian reads

$$\mathcal{H}_{\mathrm{eff}} = \frac{m_s}{2}v^2_{G\|} + \mu_s(B+\delta B) + e_s\mathcal{J}[\phi] \tag{19}$$

where $\delta B = B_0\delta(r,\theta)\cos(N_c\varphi)$

The magnetic drift $\mathbf{v}_{\mathbf{D}s}$, the electric drift $\mathbf{v}_{\mathbf{E}\times\mathbf{B}_s}$ and the parallel force $f_{\|s}$ appear when developing equations (17) and (18) such that

$$\mathbf{v}_{\mathbf{D}s} = \frac{m_s v^2_{G\|} + \mu_s B}{e_s B^\star_\|}\frac{\mathbf{B}\times\boldsymbol{\nabla}B}{B^2}, \tag{20}$$

$$\mathbf{v}_{\mathbf{E}\times\mathbf{B}_s} = \frac{\mathbf{B}\times\boldsymbol{\nabla}\bar{\phi}}{BB^\star_\|}, \tag{21}$$

$$f_{\|s} = -\mu_s(\mathbf{b}^\star_{\mathbf{s}}\cdot\boldsymbol{\nabla})B, \tag{22}$$

the motion equations of GYSELA are then modified as follows

$$\frac{d\mathbf{x}_G}{dt} = v_{G\|}\mathbf{b}^\star{}_s + \mathbf{v}_{\mathbf{D}s} + \delta\mathbf{v}_{\mathbf{D}s} + \mathbf{v}_{\mathbf{E}\times\mathbf{B}_s} \tag{23}$$

$$m_s\frac{dv_{G\|}}{dt} = f_{\|s} + \delta f_{\|s} - e\mathbf{b}^\star_{\mathbf{s}}\cdot\boldsymbol{\nabla}\bar{\phi} + \frac{m_s v_{G\|}}{B}\mathbf{v}_{\mathbf{E}\times\mathbf{B}_s}\cdot\boldsymbol{\nabla}B \tag{24}$$

where $\mathbf{b}_s^* = \frac{1}{B_{\|s}^*}\left(\mathbf{B} + \frac{m_s v_{G\|}}{e_s B}\boldsymbol{\nabla}\times\mathbf{B}\right)$. The new terms due to ripple and yield

$$\delta\mathbf{v}_{\mathbf{D}s} = \frac{m_s v_{G\|}^2 + \mu_s B}{e_s B_{\|}^\star}\frac{\mathbf{B}\times\boldsymbol{\nabla}\delta B}{B^2} \tag{25}$$

$$\delta f_{\|s} = -\mu_s(\mathbf{b}_\mathbf{s}^\star\cdot\boldsymbol{\nabla})\delta B \tag{26}$$

such that the magnetic ripple only adds a term $\delta\mathbf{v}_D$ to the magnetic drift and a parallel force $f_{\|s}$ in the parallel momentum conservation equation. With the notation $w_{Ds} = \frac{\mu_s}{e_s B_{\|s}^* \mathcal{J}_s B}$, the contravariant components of the new magnetic drift term $\delta\mathbf{v}_D$ are

$$\delta v_{Ds}^r = w_{Ds}\left(B_\theta\frac{\partial\delta B}{\partial\varphi} - B_\varphi\frac{\partial\delta B}{\partial\theta}\right) \tag{27}$$

$$\delta v_{Ds}^\theta = w_{Ds}B_\varphi\frac{\partial\delta B}{\partial r} \tag{28}$$

$$\delta v_{Ds}^\varphi = -w_{Ds}B_\theta\frac{\partial\delta B}{\partial r}. \tag{29}$$

The parallel force $f_{\|s}$ reads

$$f_{\|s} = -\mu_s\left(\frac{\partial\delta B}{\partial r}b_s^{*r} + \frac{\partial\delta B}{\partial\theta}b_s^{*\theta} + \frac{\partial\delta B}{\partial\varphi}b_s^{*\varphi}\right)$$

where the contravariant coordinates of $\mathbf{b}_\mathbf{s}^\star$ read

$$b_s^{*i} = (\mathbf{b}_s^*\cdot\boldsymbol{\nabla})x_G^i = \frac{1}{B_{\|s}^*}\left(B^i + \frac{m_s v_{G\|}}{e_s}\frac{(\boldsymbol{\nabla}\times\mathbf{B})^i}{B}\right)$$

or more specifically

$$b_s^{*r} = 0 \quad ; \quad b_s^{*\theta} = \frac{B^\theta}{B_{\|s}^*} \quad ;$$
$$b_s^{*\varphi} = \frac{1}{B_{\|s}^*}\left(B^\varphi + \frac{m_s v_{G\|}}{e_s}\frac{(\boldsymbol{\nabla}\times\mathbf{B})^\varphi}{B}\right).$$

In practice, $\frac{\partial\delta B}{\partial r}$ and $\frac{\partial\delta B}{\partial\theta}$ are negligible compared to $\frac{\partial\delta B}{\partial\varphi}$. Consequently, only $\frac{\partial\delta B}{\partial\varphi}$ has been added to the code to avoid unnecessary additional calculations and increased simulation time. The following sections are dedicated to the verification and validation of this implementation.

5. Verification through toroidal angular momentum conservation

From now on, only a single ion species is considered so the subscript s is omitted. To verify the implementation of the ripple perturbation in GYSELA, a scan in ripple amplitude is performed to check the conservation of toroidal angular momentum. One of the major effects of a non-axisymmetric magnetic perturbation is an additional toroidal torque: the magnetic drag $\mathcal{M}$. The flux surface averaged angular momentum conservation [31] involves this new term:

$$m\frac{\partial\langle nRV_T\rangle}{\partial t} = -\langle\nabla\cdot\Pi_\varphi\rangle - \langle T_\varphi\rangle + \langle\boldsymbol{J}\cdot\boldsymbol{\nabla}\psi\rangle + \langle\mathcal{M}\rangle \tag{30}$$

where $V_T = \frac{1}{n}\int d^3v\left\{v_\|(B_\varphi/B)F\right\}$ is the gyrocenter mean toroidal velocity (B_φ is the toroidal component of the magnetic field), Π_φ the toroidal Reynolds stress, T_φ a polarization term, J the sum of radial currents due to the magnetic and electric drifts respectively and ψ the poloidal magnetic flux normalized to (-2π).

Boundary physics, inevitably present either in global codes or in experiments, acts as a momentum sink which is not included in the analytical model. For this reason, the considered profile of the ripple amplitude in the following simulations is taken radially gaussian and maximum at mid-radius. Also, no poloidal dependence is accounted for. It reads $\delta_{\text{sim}} = \delta_0 e^{-32(r/a-0.5)^2}$ with δ_0 the mid-radius ripple amplitude. The usual way to perform simulations for neoclassical studies is to artificially filter out all toroidal Fourier modes of the electric potential ϕ except the axisymmetric component. This cannot be done here as ripple adds toroidal harmonics with N_c periodicity. The chosen solution to avoid turbulence is then to initiate the simulations below the instability threshold, i.e. with a sufficiently weak temperature gradient. It is also verified that ripple-induced mode amplitudes are low enough such that the inequality $e\phi_{kN_c} \ll \mu B_{kN_c}$, with $k = 1, 2, \ldots$, is satisfied, which ensures that the hamiltonian considered in the reduced model is a relevant approximation for those cases. The parameters of the simulations are summarized in table 2.

Table 2. Simulation parameters. L_N and L_T are the density and temperature gradient's length, ρ_i is the ion Larmor radius.

Species	Deuterium
Aspect ratio R_0/a	3.2
Safety factor	$q = 0.854 + 2.184(r/a)^2$
Density gradient	$R_0/L_N = 6$
Temperature gradient	$R_0/L_T = 6$
Collisionality at $r/a = 0.5$	$\nu^\star = 0.1$
ρ_i/a at $r/a = 0.5$	$\rho^\star = 1/150$
Number of coils	$N_c = 16$

Four simulations using different ripple amplitudes are analyzed. The lhs of equation (30), which is a standard output of GYSELA, is compared with the sum of the contributions in the rhs for each simulation. The radial profiles of these quantities are plotted in figure 5 and show a satisfactory agreement for all ripple amplitudes attesting good momentum conservation in the code. The negligible disparity between plain and dashed lines is a measure of the numerical error in the code. Without turbulence, magnetic braking quickly becomes the dominant contribution as indicated in figure 6 that shows the radial profile of the rhs terms of the toroidal torque conservation. This torque induced by ripple then drives the mean toroidal velocity. The implementation of a ripple magnetic perturbation being successful, the code GYSELA can be confronted to the analytical neoclassical reduced model and NEO.

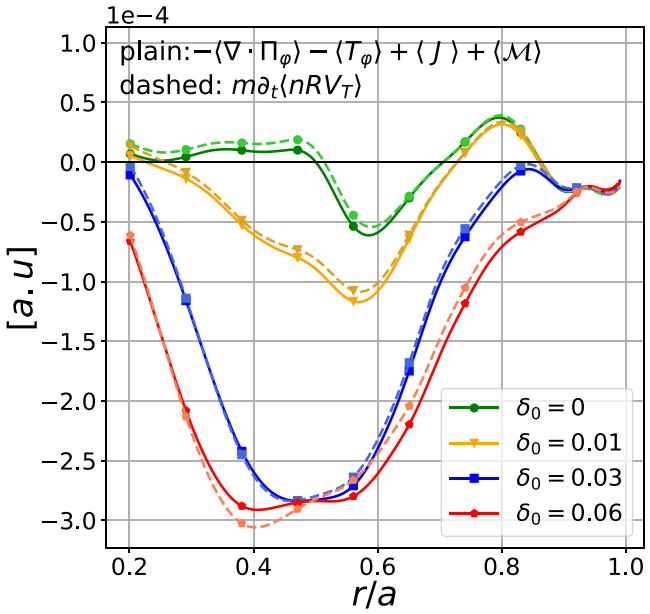

Figure 5. Radial profile of the time derivative of toroidal angular momentum (dashed) and the sum of the expected contributions (plain) for different radially gaussian ripple amplitudes such that $\delta_{\rm sim}(r) = \delta_0 \exp[-32(r/a-0.5)^2]$ at $t = 32500$ $[\omega_{c0}^{-1}]$.

6. Comparison of GYSELA global simulations with neoclassical predictions and NEO

In this section, the ability of GYSELA to assess neoclassical processes is tested against two different tools. The first one is the aforementioned reduced model. The other one is the drift kinetic solver NEO which captures all the neoclassical physics. A perfect benchmark would compare all the transport matrix coefficients from both codes and the model for a wide range of δ/ε, $\nu^\star$ and $N_c q$. However, it would require a too large quantity of simulations and a subsequent post-treatment.

The comparison between the reduced model, GYSELA and NEO is performed in the range of collisionalities $\nu^\star \in [0.05$–$0.5]$ and for three ripple amplitudes: $\delta = 0.5\%$, $\delta = 1\%$ and $\delta = 3\%$ at $\varepsilon = 0.16$ and at a fixed $N_c q = 1.4 \times 16$. Figure 7 shows a $\nu^\star$ scan of k_{V_T} for those three ripple amplitudes obtained with GYSELA, NEO and the reduced model. A fair agreement is found between GYSELA and NEO, where the average relative error is less than 10%. These results show that the model collision operator used in GYSELA is well designed to describe neoclassical processes in the collisionality range $\nu^\star \in [0.05, 0.5]$. Agreement between both codes and the neoclassical model in non-axisymmetric configurations is also obtained regarding the thermal drives. However the $\delta = 0.5\%$ case with GYSELA does not seem to undergo the $1/\nu^\star$ trend followed by the model and NEO. One possible explanation is that this is the only case not dominated by $Y < 1$ regimes (cf section 3). In other words, only this case is dominated by the effect of banana-trapped particles. The point is that at low $\nu^\star$, other regimes affecting only banana trapped particles exist [28, 32, 33]. They are sometimes labeled *super-banana* regimes, and correspond to the effect of higher order electric and magnetic drifts at bounce points, negligible at higher collisionalities. These regimes are not included in the present reduced model, nor in the present NEO simulations. However they are treated by GYSELA, which could explain this discrepancy at low collisionality. Note that NEO can actually compute those drifts [34]. This option was not switched on as the methodology here used to retrieve k_{V_T} in NEO is not compatible if those drifts are activated. However, a few tests with reasonable parameters for those drifts were performed in NEO and showed a reduction of k_{V_T} even for collisionality around $\nu^\star \approx 0.1$. Furthermore, the discrepancy at high $\nu^\star$ also observed at $\delta = 0.5\%$ between GYSELA and NEO is higher than for other cases. This mismatch is likely due to a numerical inaccuracy enhanced by the fact that, when the ripple amplitude decreases, the system approaches the axisymmetry degenerate limit where the toroidal velocity cannot be predicted separately from the radial electric field (cf discussion in section 2). This benchmark then indicates that one should be cautious when using GYSELA in the low ripple amplitude and high collisionality limits for simulations without turbulence. Let us note however that turbulence removes this degeneracy thanks to a turbulent toroidal viscosity.

Overall, the model which is derived in the large aspect ratio limit $\varepsilon \ll 1$ is showing a fair agreement with NEO. Alleviating this latter limit actually already modifies neoclassical predictions in the axisymmetric case quite substantially. In fact, for the axisymmetric neoclassical theory, i.e. without ripple, the finite aspect-ratio corrections [35] can change $k_{V_P} = 1.17$ to $k_{V_P} \sim 0.6$ for $\varepsilon = 0.17$ as observed in GYSELA [36]. To our knowledge, there is no analytical derivation of the aspect ratio correction for the neoclassical theory with ripple. The agreement is then unexpectedly good, especially at high δ/ε where the condition $Y < 1$ dominates.

The benchmark on the toroidal friction is shown in figure 8. Both expressions derived in section 2, i.e. ν_φ and $\nu_\varphi^{\Gamma_N=0}$ are displayed on this figure. It was expected that the expression with the zero particle flux assumption, i.e. $\nu_\varphi^{\Gamma_N=0}$, should be the best approximation as the electron are adiabatic in these simulations. However, it appears that the toroidal friction obtained in GYSELA is about 5–10 times lower than $\nu_\varphi^{\Gamma_N=0}$. The expression of the neoclassical friction obtained by considering a finite particle flux however is in reasonable agreement with GYSELA. The reason for this behavior is still an open issue.

7. Impact of ripple on the poloidal velocity

On the basis of the previous section, our reduced model in the presence of non-axisymmetric perturbations captures well the collisional processes in a broad range of collisionalities that roughly encompasses $\nu^\star \in [10^{-2}, 1]$. Except for the very edge of the plasma, likely dominated by wall interactions and orbit losses, this range is relevant for tokamaks. As mentioned in section 3, an unexpected result of the model is the effect of neoclassical processes with ripple on the thermal drive of the poloidal velocity k_{V_P}. Figure 9 shows the $k_{V_P} = \frac{eB_T}{\nabla T} V_{P,\rm eq}$ dependency with δ/ε in the $\nu^\star$ range of interest for $\nu^\star = 0.05$

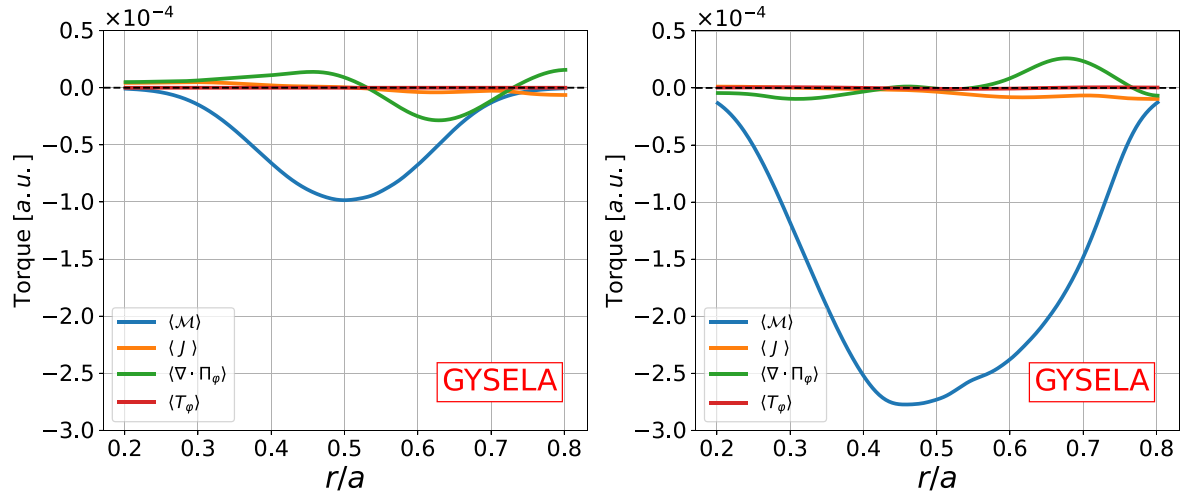

(a) $\delta_0 = 0.01$ (b) $\delta_0 = 0.03$

Figure 6. Radial profile of each term that composes the toroidal angular momentum conservation for two simulations with radially gaussian ripple amplitudes such that $\delta_{\rm sim}(r) = \delta_0 \exp[-32(r/a-0.5)^2]$ at $t = 32500$ $[\omega_{c0}^{-1}]$.

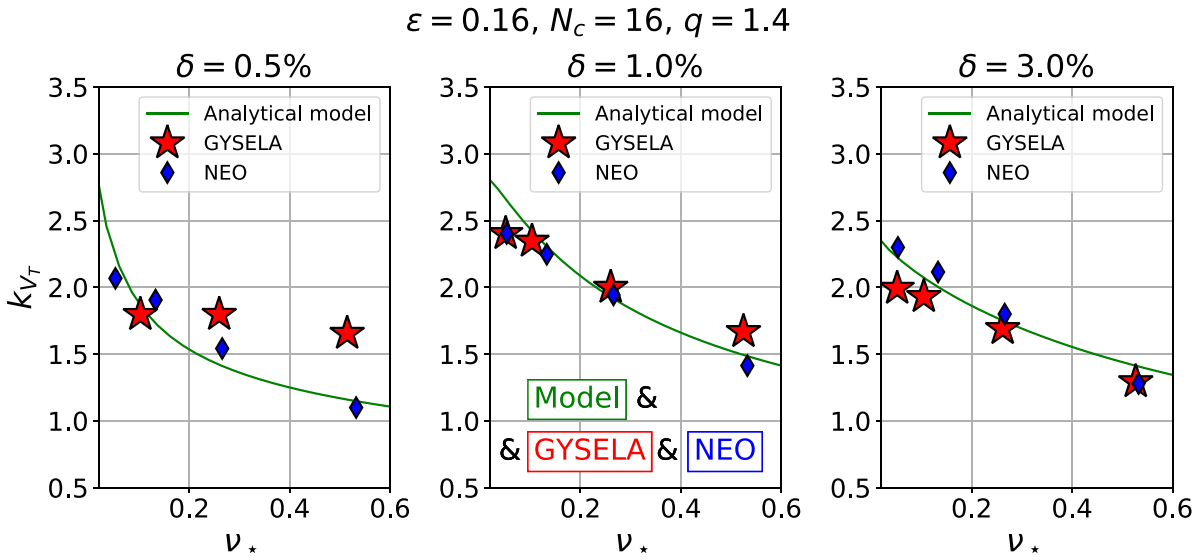

Figure 7. Collisionality scan of k_{V_T} obtained with the reduced model, GYSELA and NEO for $\delta = 0.5\%$ (left), $\delta = 1\%$ (middle) and $\delta = 3\%$ (right) at fixed $\varepsilon = 0.16$ and $N_c q = 16 \times 1.4$.

and $\nu_\star = 0.5$ obtained with the model and with the NEO code. Both recover the same trend, even though there is a disparity presumably due to the finite aspect-ratio corrections accounted in NEO but not the model.

Values of k_{V_P} at $\delta/\varepsilon = 10^{-2}$ approach the predictions of the axisymmetric neoclassical theory (in particular, $k_{V_P} = 1.17$ in the banana regime at low $\nu^\star$, cf table 1). At larger δ/ε, k_{V_P} is found to decrease, with a sharp drop off around $\delta/\varepsilon \sim 4.10^{-2}$. It can even reverse sign at low collisionality and become negative at $\delta/\varepsilon \sim 2.10^{-1}$, meaning that the poloidal velocity itself could change sign. This observation is surprising, as the classical asymptotic limits at low collisionality defined in table 1 predict that k_{V_P} can become negative only when $\delta > \varepsilon$. This conundrum is solved when refining the asymptotic limit to different classes of particle energy. Defining the normalized energy $u = (v_\perp/V_{\rm thi})^2$ with $v_\perp$ the particle velocity component perpendicular to magnetic field lines, it is indeed possible to show that the previous criterion on the ripple amplitude applies for particles of energy $u > (\delta/\varepsilon)^{-3/2}\nu^\star/(N_c q)$. However, for particles of lower energy, the criterion actually reads $\delta > \varepsilon\nu^\star(N_c q)^{-1/2}$ which is reached at way lower ripple amplitudes. In our simulations, this criterion roughly applies for particles of energy $u < \nu^\star$ which concern a non-negligible fraction of total particles.

To ensure the validity of this result, some gyrokinetic simulations with the GYSELA code were run with different ripple amplitudes. As mentioned in section 6 and appendix B, reaching a neoclassical equilibrium in gyrokinetic simulations is

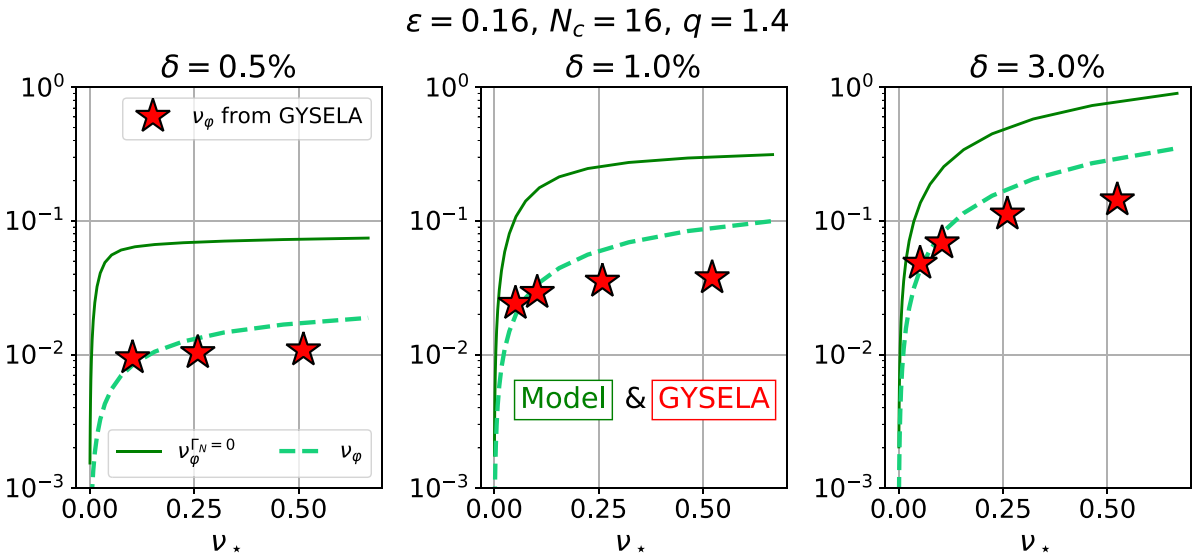

Figure 8. Collisionality scan of ν_φ and $\nu_\varphi^{\Gamma_N=0}$ obtained with the reduced model and GYSELA for $\delta = 0.5\%$ (left), $\delta = 1\%$ (middle) and $\delta = 3\%$ (right) at fixed $\varepsilon = 0.16$ and $N_c q = 16 \times 1.4$.

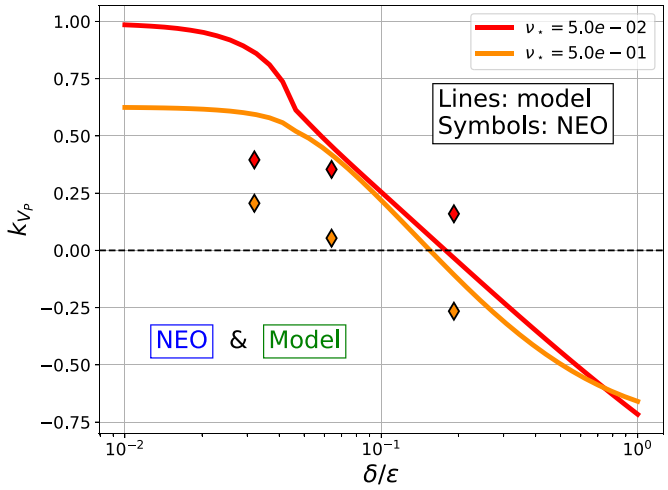

Figure 9. Scan in ripple amplitude of thermal drive k_{V_P} obtained with the reduced model and NEO for different collisionalities $\nu^\star$ at $N_c q = 16 \times 1.4$.

challenging. Indeed, the characteristic time for the system to reach such an equilibrium is of the order of the energy confinement time. Simulations that long would be numerically expensive and all the thermodynamical gradients would evolve significantly. Consequently, no equilibrium would be reached until density and temperature profiles are flat. For this reason, simulations are here used only to get a trend on the poloidal velocity evolution. The simulation parameters are the same as in table 2. The initial poloidal velocity profile is flat and set to zero. Figure 10(a) then shows the radial profile of the poloidal velocity at $\omega_c t = 5.10^4$ for ripple amplitude profiles displayed figure 10(b). For the axisymmetric case, i.e. without ripple, V_P is essentially diamagnetic and thus follow the pressure gradient. With ripple, it appears that V_P increases significantly and monotonously with the δ/ε value. This effect is particularly strong for the 'Gaussian 3%' case near mid-radius and the Tore Supra case near plasma edge. Again, this figure only shows a trend and not accurate results since, for example, the temperature profile is not exactly the same in each simulation as the neoclassical heat flux (not discussed in this paper) is also modified by ripple and consequently temperature evolves differently for each case. However a clear effect on the poloidal velocity is identified.

To get a more accurate idea of the effect of ripple in a realistic plasma, simulations involving more physics were run. They involve ITG turbulence, a heat source keeping a steady temperature profile and the presence of a limiter [37]. The main simulation parameters at $r/a = 0.5$ are $\rho^\star = 1/250$, $\nu^\star = 0.1$, $R_0/L_T = 8$, $R_0/L_N = 2.2$ and $q = 1.4$. Figure 11 shows the radial profiles of the coarse-grained poloidal velocity V_P for a case without ripple and another with the Tore Supra ripple perturbation. The coarse-graining procedure consists in a temporal averaging between $6.10^4 < \omega_c t < 9.10^4$ and a radial sliding average with a window of about $50\rho_i$. This procedure aims at smoothing the large fluctuations that appear in the presence of turbulence. As previously, these simulations are not fully converged as reaching an equilibrium would require excessive numerical resources. However, they provide reliable hints as to the long term behavior of flows. As for the neoclassical cases discussed just before, the poloidal velocity without ripple is mainly diamagnetic up to an offset due to turbulent contributions. The case with the Tore Supra ripple amplitude displays the same increasing of V_P seen in figure 10(a). It shows that a realistic magnetic configuration could lead to V_P being affected strongly at the edge and mildly at mid-radius. The fact that realistic ripple impacts plasma this far from edge is a consequence of the δ/ε ratio which is not negligible near mid-radius. Ripple contribution to the poloidal velocity is then significant, especially at the plasma edge.

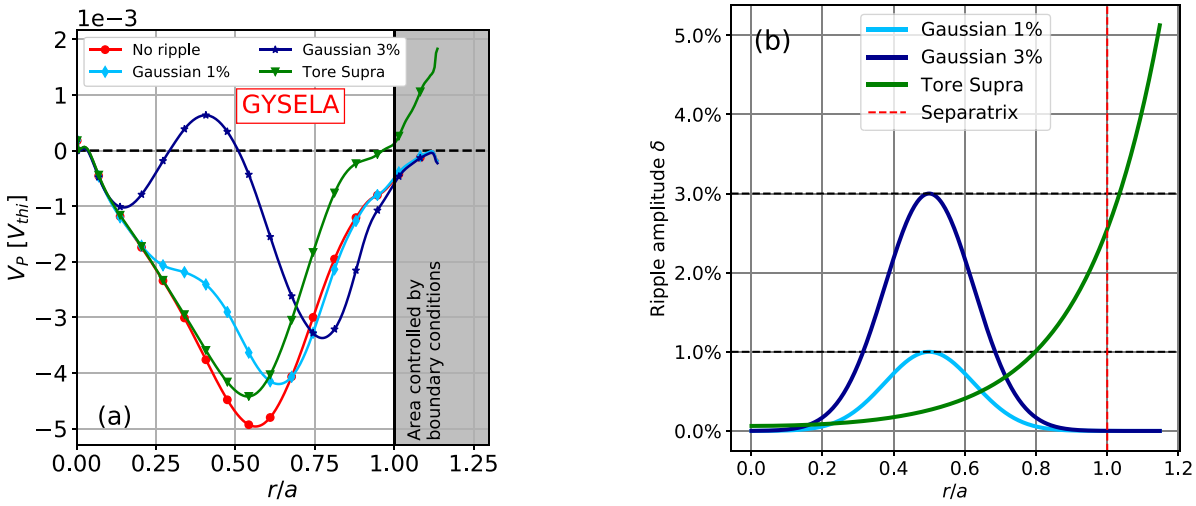

Figure 10. (a) Radial profile of poloidal velocity at $\omega_c t < 5.10^4$ for the poloidally averaged ripple amplitudes in (b). Velocity is normalized to the ion thermal velocity V_{thi} in GYSELA.

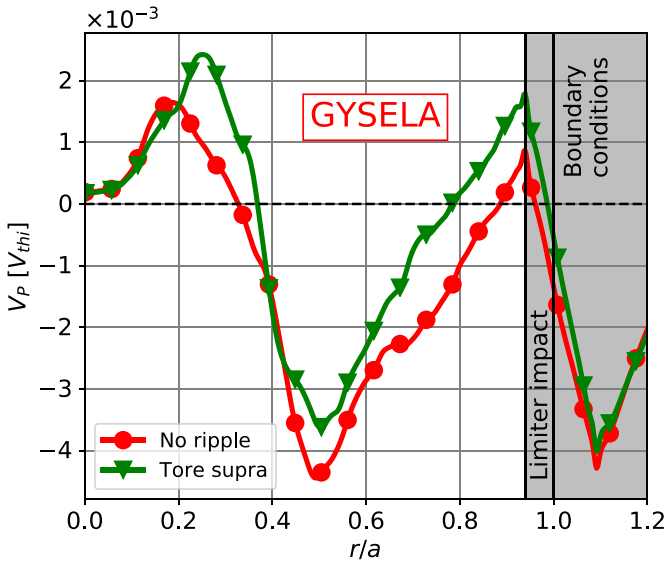

Figure 11. Radial profile of the coarse-gained poloidal velocity obtained in GYSELA simulations of ITG turbulence in the axisymmetric case (red) and for the Tore Supra ripple (green).

8. Conclusion

Magnetic ripple perturbations have been successfully implemented in GYSELA by modifying the effective hamiltonian. Key verification has been achieved through toroidal angular momentum conservation where a new term, the magnetic drag due to the ripple perturbation, becomes the dominant contribution at large ripple amplitude. GYSELA results have been benchmarked regarding the neoclassical processes occurring in presence of ripple thanks to an analytical neoclassical model and the NEO code. This study is a primordial step in order to pinpoint the range of parameters where the code is reliable. Good agreement with the NEO code is found, meaning GYSELA is able to properly describe ripple-induced neoclassical processes down to relatively low collisionality $\nu^\star \sim 0.05$. GYSELA results are also found to well agree with the model which is derived in the low collisionality and large aspect ratio limit.

In addition to the benchmark, one remarkable result of the model, which is recovered in GYSELA simulations, is the change of sign of the poloidal velocity when increasing the ripple amplitude. Such behavior was expected only for extremely (unrealistic) large values of ripple amplitude. Our findings show that the neoclassical contribution to the poloidal velocity is likely to change direction already at moderate ripple amplitudes. These conditions are expected to be met at the edge of tokamak plasmas like WEST.

Data availability statement

All data that support the findings of this study are included within the article (and any supplementary files).

Acknowledgments

The authors wish to thank E Belli for useful discussions and support. This work has been carried out within the framework of the EUROfusion Consortium, funded by the European Union via the Euratom Research and Training Programme (Grant Agreement No. 101052200—EUROfusion). Views and opinions expressed are however those of the author(s) only and do not necessarily reflect those of the European Union or the European Commission. Neither the European Union nor the European Commission can be held responsible for them. This work was performed using HPC resources from CINECA. This work was supported by funding from the European Union's Horizon 2020 research and innovation program under Grant Agreement No. 824158 (EoCoE II).

Appendix A. Explicit expression of the transport matrix coefficients

This section gives the details of the terms that appears in the transport matrix in section 2. In the general case the ripple perturbation amplitude δ depends on (r,θ). It is useful to separate this amplitude in a poloidal average $\bar{\delta}(r) = \int \frac{d\theta}{2\pi}\delta(r,\theta)$ and a poloidal modulation $\tilde{\delta}(r) = \delta(r,\theta)/\bar{\delta}$.

The transport matrix is symmetrical. Its six independent elements are given by the following expressions:

$$d_n = \int_0^{+\infty} du \left(u - \frac{3}{2}\right)^n \mathcal{K}(u) \tag{A.1}$$

$$\tilde{d}_n = \int_0^{+\infty} du \left(u - \frac{3}{2}\right)^n \tilde{\mathcal{K}}(u) \tag{A.2}$$

$$\hat{d}_n = \int_0^{+\infty} du \left(u - \frac{3}{2}\right)^n \hat{\mathcal{K}}(u) \tag{A.3}$$

where

$$\mathcal{K}(u) = \sqrt{\frac{\pi}{2}} e^{-u} u^2 K_{tor,I}(r,u) \tag{A.4}$$

$$\tilde{\mathcal{K}}(u) = \frac{32}{9}\left(\frac{2}{\pi}\right)^{3/2}\left(\frac{\bar{\delta}}{\varepsilon}\right)^{3/2}\frac{G_1}{\nu^\star} e^{-u}u^{5/2}\frac{1}{\bar{\nu}(u)} \tag{A.5}$$

$$+2\left(\frac{2}{\pi}\right)^{3/2}\frac{1}{N_b q}\left(\frac{\bar{\delta}}{\varepsilon}\right)^2\frac{1}{\nu^\star}\left[1 - H(u-u_c)\right] \times e^{-u}u^{5/2}\frac{1}{\bar{\nu}(u)}K_{rip,II}(r,u) \tag{A.6}$$

$$+\sqrt{\frac{\pi}{2}}N_b q\left(\frac{\bar{\delta}}{\varepsilon}\right)^2 H(u-u_c)\, e^{-u}u^2 K_{st}(r,u) \tag{A.7}$$

$$\hat{\mathcal{K}}(u) = \sqrt{\frac{\pi}{2}}\left(N_b q\right)\left(\frac{\bar{\delta}}{\epsilon}\right)^2 e^{-u}u^2 K_{rip,I}(r,u) \tag{A.8}$$

where H is the Heaviside function.

The normalized collision frequency [38] is defined as:

$$\bar{\nu}(u) = \frac{3}{4}\sqrt{2\pi}\frac{1}{u^{3/2}}\left(\Phi(u^{1/2}) - G(u^{1/2})\right)$$
$$\text{where } \begin{cases} \Phi(u) = & \frac{2}{\sqrt{\pi}}\int_0^u dx \exp\left(-x^2\right) \\ G(u) = & \frac{1}{2u^2}\left(\Phi(u) - u\frac{d\Phi(u)}{du}\right). \end{cases}$$

The functions K provide smooth transitions between various collision regimes:

$$K_{rip,I}(r,u) = \min\left(G_0', G_0''\frac{4}{\pi}\mathcal{I}\frac{\nu^\star}{N_c q}\left(\frac{\varepsilon}{\bar{\delta}}\right)^{3/2}\frac{\bar{\nu}(u)}{u^{1/2}}\right) \tag{A.9}$$

$$K_{tor,I}(r,u) = \min\left(1, \frac{4}{\pi}\mathcal{I}\nu^\star\frac{\bar{\nu}(u)}{u^{1/2}}\right) \quad \text{with } \mathcal{I} = 1.38 \tag{A.10}$$

$$K_{rip,II}(r,u) = 1 + \frac{\pi^2}{8}\nu^\star (N_c q)^2\frac{\bar{\nu}(u)}{u^{1/2}} \tag{A.11}$$

$$K_{st}(r,u) = \left(1 + \frac{1}{\sqrt{\pi}}\frac{m v_{th}}{eB_0}\left(\frac{N_c q}{\varepsilon}\right)^{3/2}\frac{dq}{dr}\bar{\delta}u^{1/2}\right)^{-1} \tag{A.12}$$

where is defined the continuous functions $\min(x,y) = \frac{xy}{x+y}$.

The so-called form factors G_0', G_0'', G_1, used to discriminate banana trapped particles and magnetic wells, are given by the relations:

$$G_0'(r) = \int_{Y<1}\frac{d\theta}{2\pi}\tilde{\delta}^2(r,\theta)$$
$$G_0''(r) = \int_{Y<1}\frac{d\theta}{2\pi}\tilde{\delta}^{\frac{1}{2}}(r,\theta)$$
$$G_1(r) = \int_{Y<1}\frac{d\theta}{\pi}\tilde{\delta}^{\frac{3}{2}}(r,\theta)\sin^2\theta \tag{A.13}$$

where $Y(r,\theta) = \frac{\varepsilon|\sin\theta|}{N_c q\delta} < 1$ is the condition of existence of ripple-induced magnetic wells.

The transition between neoclassic and stochastic regimes is considered through the following limit in energy:

$$u_c = \frac{R_0}{8\pi}\left(\frac{dq}{dr}\right)^{-1}\left(\frac{mV_{\text{thi}}}{eB_0}\right)^{-2}\frac{q^{-5/2}}{N_c^{3/2}}\frac{\varepsilon^3}{\bar{\delta}} \tag{A.14}$$

Appendix B. Specific methodology to retrieve k_{V_T} and $\hat{\nu}_\varphi$ in GYSELA and NEO

As the neoclassical theory gives the transport matrix, the quantity to compare between codes and reduced model are the (d_{ij}) coefficients in GYSELA and NEO which only depend on δ/ε, $\nu^\star$ and $N_c q$. Then, given the structure of equation (2), one could determine those coefficients if enough (A_N, A_{V_T}, A_T) and $(\Gamma_N, \Gamma_{V_T}, \Gamma_T)$ sets were known. In theory, only three sets would suffice for a given $(\delta/\varepsilon, \nu^\star, N_c q)$ set. However the least-square method used as linear solver proved to be inefficient and would probably need more statistics. In addition, the benchmark aims at verifying the range of validity of the theory for a wide range of ripple amplitudes and collisionalities. As discussed below, obtaining a set $(A_N, A_{V_T}, A_T, \Gamma_N, \Gamma_{V_T}, \Gamma_T)$ linked to one combination of $(\delta/\varepsilon, \nu^\star, N_c q)$ basically amounts to running one simulation. The number of simulations required to retrieve all the matrix coefficient would then be enormous. Instead, only the thermal drives k_{V_T}, k_N and k_{V_P} (defined in section 3 are benchmarked.

B.1. The GYSELA code

In GYSELA, the main difficulty lies in the boundary conditions that can add extra effects not taken into account in the reduced model like orbit losses, momentum flux carried by waves or scrape-off layer interactions. For this reason, a radially gaussian ripple, as used in section 5, is considered. The radial location of interest is then chosen at $r/a = 0.5$. In GYSELA, (A_{V_T}, A_T) are inputs and Γ_{V_T} is an output.

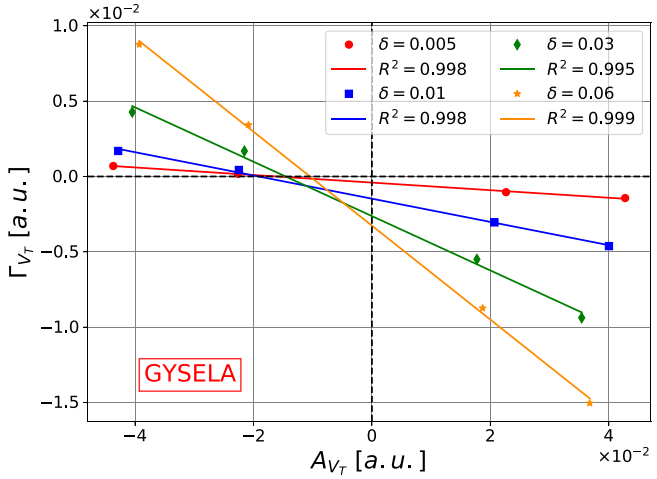

Figure B1. Magnetic braking force Γ_{V_T} versus A_{V_T} for different ripple amplitudes δ. Each point corresponds to a simulation with different initial toroidal velocity profiles and represents the (A_{V_T}, Γ_{V_T}) retrieved at $r/a = 0.5$ after the GAMs at $\nu^\star = 0.1$.

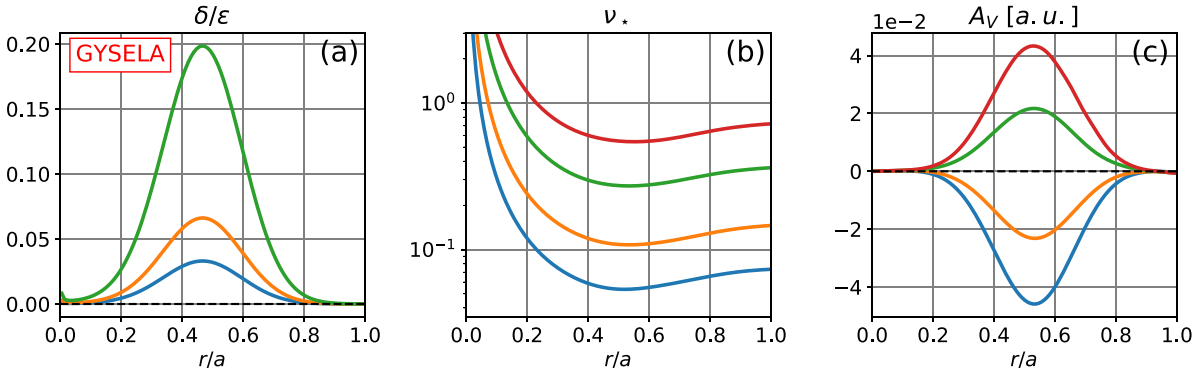

Figure B2. Initial radial profiles of the effective ripple amplitudes δ/ϵ (a), the collisionalities $\nu^\star$ (b) and the normalized toroidal velocities A_{V_T} (c) used for the scan.

The temperature gradient A_T evolves slowly compared with A_{V_T} and Γ_{V_T}. In all simulations, A_T is then fixed at the same value and only the initial A_{V_T} profile is changed. This makes the numerical resolution even simpler and more robust, as a linear regression on $\Gamma_{V_T}(A_{V_T})$ gives ν_φ and k_{V_T} which are respectively associated to the slope and intersection with the x-axis. A (A_{V_T}, Γ_{V_T}) set is retrieved after the GAM phase which is here longer than a few collision times in each simulation, the characteristic time needed for neoclassical effects to establish. This is illustrated in figure B1 obtained thanks to 16 simulations with four different ripple amplitudes, four toroidal velocities, and a single $\nu^\star$ profile.

This exercise has been done for four collisionality profiles for a total of 48 gyrokinetic simulations. All the input profiles are showed in figure B2.

B.2. The NEO code

NEO is an Eulerian local code that solves the drift-kinetic equation with a linearized full Fokker-Planck collision operator [9, 10]. It is considered as a reference code for neoclassical predictions. The only approximation is the so-called *drift-ordering* $\rho^\star \ll 1$. As NEO is able to handle non-axisymmetric flux surface (see [34] for more details), the following simulations uses the same ripple perturbations used in GYSELA. NEO has to be benchmarked in similar regime to GYSELA for the benchmark. This require zero particle flux $\Gamma_N = 0$, as imposed by the adiabatic electron response in GYSELA. However, contrary to the axisymmetric version, here NEO does not enforce ambipolarity so that $\Gamma_N \neq 0$ in the general case. Notice that, according to equation (30) at equilibrium, the $\Gamma_N = 0$ condition also imposes $\Gamma_{V_T} = 0$, hence $V_T = k_{V_T} \nabla T / eB_P$ which is an output in NEO. It follows that, in such regime, this methodology does not allow one to retrieve the neoclassical toroidal friction ν_φ with NEO. To retrieve k_{V_T}, one must first find an input set of (A_N, A_T) for which $\Gamma_N = 0$. There is no quasi-neutrality constraint in NEO, and consequently no onset of non-linearity, even small, due to the electric potential as in GYSELA. For this reason, the relation between (A_N, A_T) and $(\Gamma_N, \Gamma_{V_T}, \Gamma_T)$ is linear in NEO. Taking advantage of this, A_N is set at a constant value while a scan on A_T is performed. The resulting outputs of interest, i.e. Γ_N, Γ_{V_T} and A_{V_T} then exhibit a linear dependency with respect to A_T, cf figure B3.

Note that this method could also have been done by performing a scan on A_N at fixed A_T. The $\Gamma_N = 0$ condition is

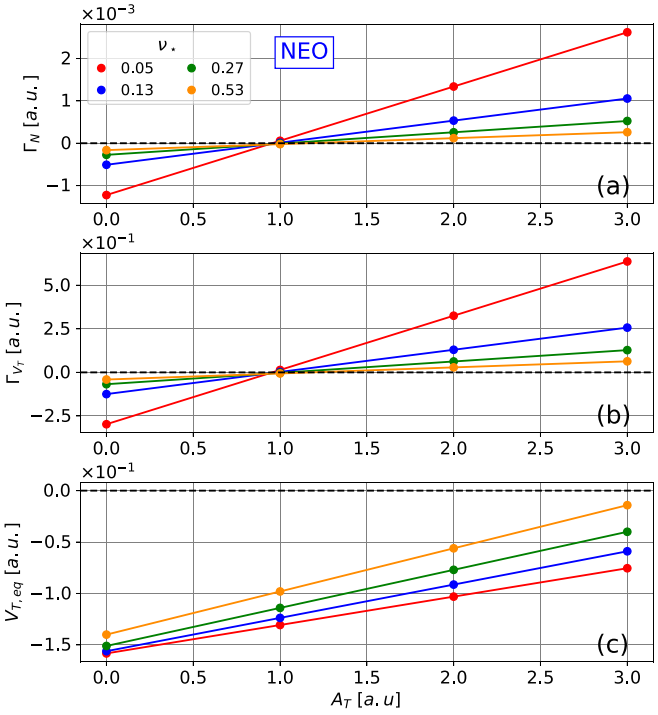

Figure B3. From NEO simulations: Equilibrium particle flux $\Gamma_{\rm eq}$ (a), magnetic braking force $\mathcal{M}_{\rm eq}$ (b) and mean toroidal velocity $V_{T,\rm eq}$ (c) for different collisionalities $\nu^\star$ at fixed $\delta/\varepsilon = 0.03/0.16$ and $N_c q = 16 \times 1.4$ over a wide range of A_T.

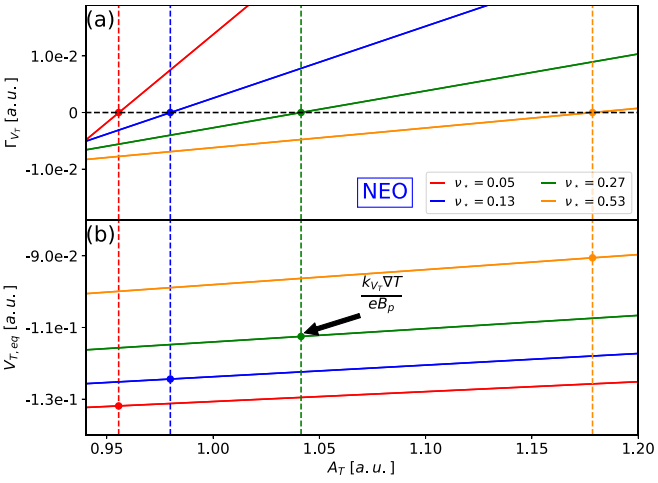

Figure B4. From NEO simulations: Magnetic braking force $\mathcal{M}$ (a) and the toroidal velocity V_T (b) for different collisionalities $\nu^\star$ at fixed $\delta/\varepsilon = 0.03/0.16$ and $N_c q = 16 \times 1.4$. The value of V_T at A_T for which $\mathcal{M}$ cancels is directly linked to the neoclassical thermal drive k_{V_T}.

then obtained by drawing the $\Gamma_N(A_T)$ line using a few points, each obtained with one simulation, and by retrieving the A_T value that cancels the particle flux. At this value $\Gamma_{V_T} = 0$ as expected and already discussed, so the output toroidal velocity is equal to $A_{V_T} = k_{V_T} A_T$. This provides the value of k_{V_T}. Figure B4 illustrates this procedure, that is repeated for each $\nu^\star$ considered for a given ripple amplitude δ.

ORCID iDs

R Varennes https://orcid.org/0000-0001-7509-7810
X Garbet https://orcid.org/0000-0001-5730-1259
Y Sarazin https://orcid.org/0000-0003-2479-563X
P Ghendrih https://orcid.org/0000-0002-1505-6512
P Donnel https://orcid.org/0000-0002-6669-416X
K Obrejan https://orcid.org/0000-0002-1906-4181

References

[1] Fenzi C *et al* 2011 *Nucl. Fusion* **51** 103038
[2] Nave M F F, Johnson T, Eriksson L-G, Crombé K, Giroud C, Mayoral M-L, Ongena J, Salmi A, Tala T and Tsalas M 2010 *Phys. Rev. Lett.* **105** 105005
[3] Varennes R *et al* 2022 *Phys. Rev. Lett.* **128** 255002
[4] Grandgirard V *et al* 2016 *Comput. Phys. Commun.* **207** 35–68
[5] Cole A J, Hegna C C and Callen J D 2008 *Phys. Plasmas* **15** 056102
[6] Shaing K C 2003 *Phys. Plasmas* **10** 1443–8
[7] Garbet X *et al* 2010 *Phys. Plasmas* **17** 072505
[8] Grua P and Roubin J-P 1990 *Nucl. Fusion* **30** 1499–509
[9] Belli E A and Candy J 2008 *Plasma Phys. Control. Fusion* **50** 095010
[10] Belli E A and Candy J 2011 *Plasma Phys. Control. Fusion* **54** 015015
[11] Mynick H E 2006 *Phys. Plasmas* **13** 058102
[12] Goldston R J, White R B and Boozer A H 1981 *Phys. Rev. Lett.* **47** 647–9
[13] Helander P and Sigmar D J 2002 *Collisional Transport in Magnetized Plasmas* (Cambridge: Cambridge University Press)
[14] Hinton F L and Hazeltine R D 1976 *Rev. Mod. Phys.* **48** 239–308
[15] Yushmanov P 1982 *Nucl. Fusion* **22** 315–24
[16] Yushmanov P 1983 *Nucl. Fusion* **23** 1599–612
[17] Tsypin V S, Mikhailovskii A B, Galvão R M O, Nascimento I C, Tendler M, de Azevedo C A and de Assis A S 1998 *Phys. Plasmas* **5** 3358–65
[18] Shaing K C 1983 *Phys. Fluids* **26** 3315
[19] Shaing K C, Rome J A and Fowler R H 1984 *Phys. Fluids* **27** 1
[20] Shaing K C, Hirshman S P and Callen J D 1986 *Phys. Fluids* **29** 521
[21] Shaing K C 2001 *Phys. Rev. Lett.* **87** 245003
[22] Kovrizhnykh L 1984 *Nucl. Fusion* **24** 851–936
[23] Connor J and Hastie R 1973 *Nucl. Fusion* **13** 221–5
[24] Beidler C D, Kolesnichenko Y I, Marchenko V S, Sidorenko I N and Wobig H 2001 *Phys. Plasmas* **8** 2731–8
[25] Hazeltine R D 1974 *Phys. Fluids* **17** 961–8
[26] Bécoulet M *et al* 2009 *Nucl. Fusion* **49** 085011
[27] Kim K, Park J-K, Boozer A H, Menard J E, Gerhardt S P, Logan N C, Wang Z R, Kramer G J, Burrell K H and Garofalo A M 2014 *Nucl. Fusion* **54** 073014
[28] Park J-k, Boozer A H and Menard J E 2009 *Phys. Rev. Lett.* **102** 065002
[29] Sun Y, Liang Y, Shaing K C, Koslowski H R, Wiegmann C and Zhang T 2011 *Nucl. Fusion* **51** 053015
[30] Matsuoka S, Idomura Y and Satake S 2017 *Phys. Plasmas* **24** 102522
[31] Abiteboul J, Garbet X, Grandgirard V, Allfrey S J, Ghendrih P, Latu G, Sarazin Y and Strugarek A 2011 *Phys. Plasmas* **18** 082503

[32] Shaing K C, Sabbagh S A and Chu M S 2008 *Plasma Phys. Control. Fusion* **51** 035009
[33] Shaing K C, Sabbagh S A and Chu M S 2009 *Plasma Phys. Control. Fusion* **51** 055003
[34] Belli E A and Candy J 2015 *Plasma Phys. Control. Fusion* **57** 054012
[35] Kim Y B, Diamond P H, Biglari H and Callen J D 1991 *Phys. Fluids* B **3** 384–94
[36] Dif-Pradalier G *et al* 2011 *Phys. Plasmas* **18** 062309
[37] Caschera E *et al* 2018 *J. Phys.: Conf. Ser.* **1125** 012006
[38] Hirshman S P and Sigmar D J 1976 *Phys. Fluids* **19** 1532